JOURNAL OF CATALYSIS 102, 1–9 (1986)

Structural, Surface, and Catalytic Properties of Bismuth Molybdovanadates Containing Foreign Atoms[1]

III. Electron Spin Resonance and Magnetic Characterization of Iron-Containing Bismuth Molybdovanadate Catalysts

DANTE CORDISCHI, MARIANO LO JACONO, GIULIANO MINELLI, AND PIERO PORTA[2]

Centro di Studio del Consiglio Nazionale delle Ricerche (CNR) su "Struttura e Attività Catalitica di Sistemi di Ossidi" (SACSO), c/o Dipartimento di Chimica, Università "La Sapienza," 00185 Roma, Italy

Received November 19, 1985

The bulk properties of two series of solid solutions with scheelite tetragonal structure and general formula $Bi_{1-x/3}\square_{x/3-y}Me_y(V_{1-x}Mo_{x-y}Fe_y)O_4$, where Me = Bi (series I) or Me = Fe (series II), were investigated by electron spin resonance (ESR) and magnetic susceptibility measurements. The incorporation of Fe^{3+} ions with high-spin configuration into the structure of bismuth molybdovanadates gives rise to three distinct ESR signals (α, β, γ). Their presence and intensity depend on the iron content (y parameter) and even more on its location into the tetrahedral B sites (series I) or into both the tetrahedral, B, and eight-coordinated A sites (series II) of the scheelite structure. Signal α, present in both catalyst series and having $g_1 = 4.2$ and $\Delta H \cong 200$ G at room temperature, is assigned to isolated Fe^{3+} in B sites. Signal β, present only in the catalysts of series II and having $g = 2.0$, is assigned to strongly coupled Fe^{3+} ions in both A and B sites (A–O_x–B antiferromagnetic coupling type). Signal γ, being present in the series I catalysts and having $g \cong 2$ and $\Delta H = 2000$ G, is assigned to Fe^{3+} weakly coupled in B sites. Moreover, the behavior of the Weiss temperature θ for the two catalyst series and its dependence on x and y compositional parameters lead to the same conclusions about the location and dispersion of Fe^{3+} ions in the scheelite structure, as obtained by ESR. A plausible hypothesis on the mechanism through which the dispersion of Fe^{3+} occurs in the molybdovanadate systems is presented.

INTRODUCTION

A preceding paper (*1*), devoted to the preparation and X-ray structural characterization of the samples, has shown that monophasic solid solutions with the scheelite ($CaWO_4$) tetragonal structure and general formula

$$Bi_{1-x/3}\square_{x/3-y}Me_y(V_{1-x}Mo_{x-y}Fe_y)O_4$$

are formed in a wide range of composition ($0.15 \leq x \leq 0.75$ and $0 \leq y \leq x/3$), where $\square$ = cation vacancies and where Me = Bi^{3+} (series I) or Me = Fe^{3+} (series II).

The present paper will report on the ESR and magnetic characterization of the same samples with the aim of providing information about the distribution, the site symmetry, and the magnetic interactions of the Fe^{3+} ions.

EXPERIMENTAL

Catalysts. The samples were prepared by coprecipitation with ammonia from aqueous solutions of ammonium heptamolybdate, ammonium vanadate, bismuth nitrate, and iron nitrate. The complete list of catalysts, the details of preparation, and the results of the X-ray characterization are reported in Part I (*1*). In addition to the above-listed catalysts a sample with lower iron content ($y = 0.01$) was prepared specifically for the present ESR investigation.

ESR measurements. For all samples, the ESR spectra were recorded at room tem-

[1] This work has been realized with the financial contribution of the "Progetto Finalizzato (CNR) on Chimica Fine e Secondaria."

[2] To whom correspondence should be addressed.

0021-9517/86 $3.00

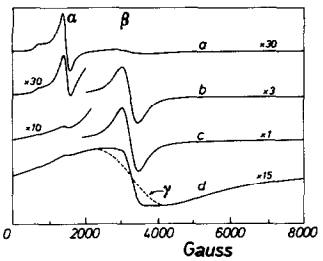

FIG. 1. ESR spectra of Fe^{3+} in $Bi_{1-x/3}\square_{x/3-y}Me_y(V_{1-x}Mo_{x-y}Fe_y)O_4$ catalysts, recorded at X-band and room temperature; samples with $x = 0.60$. Series I (*Me* = Bi): (a) with $y = 0.01$, (d) with $y = 0.1$. Series II (*Me* = Fe): (b) with $y = 0.01$, (c) with $y = 0.1$. The number on the spectra indicates the relative gain.

perature (RT) and at liquid-nitrogen temperature (LN) on a Varian E-9 spectrometer operating at X-band frequency with 100 kHz field modulation and with the standard rectangular TE_{102} resonant cavity. Relative intensities were determined from selected lines of the first derivative spectrum and/or from electronically integrated spectrum by using the Varian "Strong Pitch" as reference standard. Some selected spectra were also recorded as Q-band frequency at RT.

Magnetic susceptibility measurements. These were performed by the Gouy method at different field strengths (4, 6, and 8 kG) and in the temperature range from 78 to 300 K. A semimicrobalance reading to ±0.01 mg was employed; the apparatus was calibrated with $Hg[Co(CNS)_4]$. The samples proved to be field independent and to obey the Curie–Weiss law $\chi_{at} = C/(T - \theta)$ in the whole temperature range. The Weiss temperature θ was taken from the intercepts on the T axis of the $1/\chi_{at}$ vs T plots.

RESULTS

ESR. The bismuth molybdovanadate samples without iron ($y = 0$) do not show any ESR signal, whereas iron-containing specimens give rise to rather complex spectra. They are constituted of several signals with different shape and intensity, depending on the chemical composition and mainly on whether the iron ions are located only in the tetrahedral B cation sites (series I) or both in the tetrahedral B and the eight-coordinated A cation sites (series II) available in the scheelite structure (*1*). The component signals are described in (i), (ii), and (iii) below.

(i) As shown in Fig. 1 all the iron-containing specimens (series I and II) generate at X-band an ESR line, labeled α, at $g_1 = 4.2$ with a shoulder at $g_2 = 9.3$. This signal is typical of high-spin Fe^{3+} ions in sites of rhombic symmetry ($E/D = 1/3$); it has in fact been observed in several systems, both crystalline (*2, 3*) and amorphous (*4, 5*), and it characterizes the resonance between the middle Kramers doublet, when $h\nu/D$ is small (≤ 1) and E/D is close to 1/3 (*3*). Moreover, since this line disappears at the Q-band, it allows us to restrict the possible value of the D term to the range between 0.3 and 1.1 cm^{-1}. The shape of this signal is almost independent of the iron content and of the recording temperature; the width of the line at $g = 4.2$ in fact increases slightly with iron content, going from 185 to 220 G at room temperature and from 170 to 210 G at liquid-nitrogen temperature, when the iron content (y) varies from 0.01 to 0.2. Its intensity, I_α, follows quite well the Curie law ($I \times T$ = constant) and it is practically the same for the two series (I and II) of specimens; however, it depends on iron content. Indeed, as shown in Fig. 2, the intensity of the α signal reaches a smooth and broad maximum at y between 0.03 and 0.05, and then decreases with increasing iron content.

(ii) Besides the signal α, a second signal, labeled β, is present in the ESR spectra of specimens of series II (Figs. 1b and c), whereas it is absent or very weak in the samples of series I (Figs. 1a and d). The signal β is constituted of a single line of nearly perfect Lorentzian shape at $g = 2.00$; its linewidth is practically independent of x and y compositional parameters, but depends on the recording temperature; thus it is 440 G at RT and becomes 750 G at

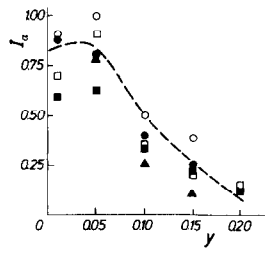

FIG. 2. Relative intensity of signal α vs y in $Bi_{1-x/3}\square_{x/3-y}Me_y(V_{1-x}Mo_{x-y}Fe_y)O_4$ catalysts. Series II (Me = Fe): (●) $x = 0.45$, (■) $x = 0.60$, (▲) $x = 0.75$. Series I (Me = Bi): (○) $x = 0.45$, (□) $x = 0.60$.

LN. The integrated intensity, I_β, does not follow the Curie law; its behavior is typical of an antiferromagnetic ensemble of spins at temperatures higher than the Néel temperature, since the produce $I \times T$ decreases from 1.00 at RT to 0.57 ± 0.05 at LN. Moreover, as shown in Fig. 3, the intensity of signal β depends strongly on both x and y: for each value of x the intensity appears to reach a maximum at about $y_{max}/2$. On the other hand, since $y_{max} = x/3$, each curve relating to any x value (from 0.15 to 0.75) reaches the maximum at $y = x/6$, and then decreases. However, only the curves corresponding to lower values of x go to zero at $y = x/3$, the others showing a tendency to decrease without reaching zero.

(iii) A third signal, labeled γ, having a very broad linewidth of ~2000 G and centered at $g = 2.0$ is present only in the ESR spectra of specimens of series I. Figure 1d shows the ESR spectrum of a sample of series I in which a weak signal β is superimposed on the signal γ. The signal γ is barely detectable at low iron content ($y \leq 0.05$) but becomes rather intense at higher y values; however, due to some scattering of the experimental data and to the relatively small number of samples examined, it was rather difficult to define accurately its dependence on both x and y. In the samples of series II the signal γ is not observed. However, in these samples the presence of a much more intense and sharp signal β, having the same g value, could hide the signal γ. Even so, the presence of signal γ under the signal β would provoke an alteration of the lineshape of the signal β. A detailed analysis of the lineshape of the signal β revealed practically no difference between concentrated ($y = 0.15$) and dilute samples ($y = 0.01$). We conclude, therefore, that in the samples of series II the signal γ is absent, or, if present, its intensity is an order of magnitude lower than the intensity of the corresponding samples of series I.

The main features of the ESR signals are reported in Table 1.

Magnetic susceptibility measurements. As reported briefly in Part I (*1*), the magnetic susceptibility measurements revealed that all samples containing iron, both series I and II, were field-independent and obeyed the Curie–Weiss law $\chi_{at} = C/(T - \theta)$. The value of the magnetic moment, μ, for all the specimens was around 5.95 B.M., and this has been taken as experimental evidence that all the iron present is in the oxidation state of 3+ and in the $3d^5$ high-spin configuration.

The dependence of the Weiss temperature, θ (which in principle may give an indication of antiferromagnetic interactions between paramagnetic ions), on the compositional parameters x and y is now presented. From an inspection of Fig. 4 some observations can be made about the behavior of θ. Both series I and II exhibit θ values different from zero, showing that antiferromagnetic interactions arise with iron content. However, at higher iron concen-

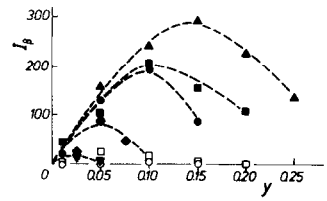

FIG. 3. Relative intensity of signal β vs y in $Bi_{1-x/3}\square_{x/3-y}Me_y(V_{1-x}Mo_{x-y}Fe_y)O_4$ catalysts. Series II (Me = Fe): (▼) $x = 0.15$, (◆) $x = 0.30$, (●) $x = 0.45$, (■) $x = 0.60$, (▲) $x = 0.75$. Series I (Me = Bi): (○) $x = 0.45$, (□) $x = 0.60$.

TABLE 1

Iron Distribution in the Height-Coordinated, A, and Tetrahedral, B, Sites of Bismuth Molybdovanadates with Scheelite Structure, and ESR Signals with Their Main Features

Specimens and ESR parameters	Iron distribution		Presence of ESR signals and their features		
	A site	B site	Signal α	Signal β	Signal γ
Series I	No	Yes	Yes	No	Yes
Series II	Yes	Yes	Yes	Yes	No
g value			4.2	2.0	~2
ΔH at RT (G)			200	440	~2000
Intensity: Curie law obeyed			Yes	No	
Intensity: Dependence			On y (Fig. 2)	On x,y (Fig. 3)	
Signal assignment			Isolated Fe^{3+} ions in B sites	Strongly coupled Fe^{3+} ions in nearby A–B sites	Weakly coupled Fe^{3+} ions in B sites

Note. Chemical formula of the catalysts: $Bi_{1-x/3}\square_{x/3-y}Me_y(V_{1-x}Mo_{x-y}Fe_y)O_4$, where $\square$ = cation vacancies, $0.15 \leq x \leq 0.75$, and $0 \leq y \leq x/3$. Series I, Me = Bi; series II, Me = Fe.

tration, these interactions are much stronger in series II, where a clear dependence, both on x and y, exists. For each value of x the variation of θ with y shows in this series two different behaviors, each one limited by a well-defined range of y.

In the first region, where y lies between zero and one-half of its maximum value ($0 \leq y \leq \frac{1}{2}y_{max}$; $y_{max} = x/3$), the values of θ increase slightly with y. It should be noted that in this region no significant difference exists between samples of the two series I and II. In the second region, where y lies between $\frac{1}{2}y_{max}$ and y_{max} ($x/6 \leq y \leq x/3$), the curve of θ vs y strongly diverges. This behavior is more evident in the samples with higher x (0.60 and 0.75).

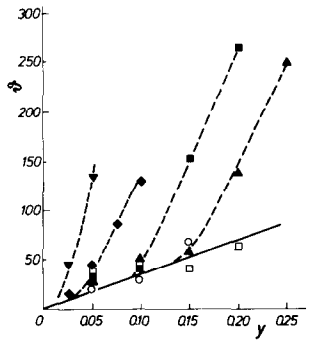

FIG. 4. Weiss temperature θ vs y in $Bi_{1-x/3}\square_{x/3-y}Me_y(V_{1-x}Mo_{x-y}Fe_y)O_4$ catalysts. Series I (Me = Bi): (○) $x = 0.45$, (□) $x = 0.60$. Series II (Me = Fe): (▼) $x = 0.15$, (◆) $x = 0.30$, (■) $x = 0.60$, (▲) $x = 0.75$.

DISCUSSION

The various ESR signals described above are assigned to Fe^{3+} ions present in the eight-coordinated A cation sites and/or in the tetrahedral B cation sites of the scheelite structure as "isolated" or "clustered" ions, where we use the latter term to denote exchange coupled ions in nearby A–B sites.

We shall first discuss the site assignment, and then the conditions in which an ion must be considered "isolated" or "clustered."

Signal assignment to Fe^{3+} ions in A or B sites. By comparing the X-ray data (*1*) and magnetic data with the ESR results, it is possible to correlate the presence of the various ESR signals with the distribution of the Fe^{3+} ions in the A and/or B sites in the

samples of series I and II. This correlation, shown in Table 1, leads to the following assignments:

(i) The signal α is due to "isolated" ions in the B sites, because it is present in all the samples and in particular in samples of series I, which have Fe^{3+} in the B sites only.

(ii) The signal β, present only in the samples of series II, is assigned to "clustered" Fe^{3+} ions located in both A and B sites.

(iii) The signal γ, present only in the specimens of series I, is attributed to weakly coupled Fe^{3+} ions in the B sites.

Magnetic interactions and scheelite structure. When a paramagnetic ion is incorporated in a diamagnetic matrix it remains "isolated" at rather low concentrations. By increasing its content, the ESR spectrum of the isolated ions is gradually replaced by a single line assigned to "clustered" ions. This is a rather general phenomenon and it has been observed in many powder systems, both crystalline (*6–13*) and amorphous (*14, 15*).

While the long-range dipole interactions provoke a broadening of the ESR spectrum without altering its main features, the exchange interactions have a stronger effect on it. Only antiferromagnetic interactions are considered here, because, as shown by the magnetic data, in the molybdovanadate system only this type of interaction is present.

By increasing the size of the exchange-coupled cluster the fine and hyperfine structure present in the spectrum of the isolated ion is progressively reduced and the spectrum collapses into a single exchange-narrowed line. It has been shown (*12, 13*) that in a powder system the clusters contributing to this line are those of size larger than two ions. The exchange-narrowed line can be observed at temperatures higher than the Néel temperature, and by lowering the temperature to near the Néel point the linewidth increases and the product $I \times T$ decreases. At a given temperature, the width, as well as the shape and the intensity of the exchange-narrowed line, depend on the

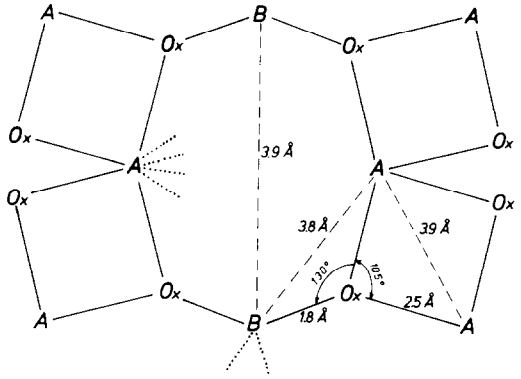

FIG. 5. Schematic representation of bonding around the tetrahedral, B, and the eight-coordinate, A, cation sites in the oxidic scheelite ABO_4 structure. Bond distances and angles are average values taken from Ref. (*17*).

strength of the exchange interactions (*16*). By considering the scheelite structure, qualitative deductions about the strength of the exchange interactions can be drawn.

As schematically shown in Fig. 5, each tetrahedral B cation site is linked, through its four oxygens, to eight nearest neighbor (n.n.) eight-coordinated A cation sites. The B–A distance and the B–Ox–A angle are ~3.8 Å and ~130°, respectively (*17*).

On the other hand the shortest A–A and B–B cationic distances are somewhat higher (~3.9 Å) than the B–A ones, each A (or B) cation site having four A (or B) cation sites as n.n.. The n.n. A cation sites are linked together by two oxygens equally distant at ~2.5 Å, with an angle A–Ox–A lower than B–Ox–A (105° as compared to 130°). It should also be noted than the n.n. B cation sites are not linked together to the same oxygen as occurs in the B–Ox–A interactions, but give rise to a long-range interaction through a B–Ox–A–Ox–B pathway.

From the above considerations it may be deduced that the strongest superexchange interactions between Fe^{3+} ions are for the A–Ox–B coupling, followed by the A–Ox–A, the weakest interaction corresponding to the B–Ox · · · B configuration.

The observed trend for the θ values, indi-

cating that antiferromagnetic interactions are stronger in the samples of series II, confirms that in this series the solid solutions contian iron in both A and B sites, whereas the samples of series I contain Fe^{3+} ions in B sites only.

The strengths of the exchange interactions between the next nearest neighbors (n.n.n.) are expected to be markedly lower than those between the n.n. sites, but, as far as their effect on the ESR spectrum is concerned, the ions must be considered "clustered" if the exchange interaction is greater than the microwave quantum used (0.31 cm^{-1} at X-band). Therefore in the range of action of the exchange forces between magnetic ions, the n.n.n. and in some cases the third nearest neighbors have frequently been included (*9–12*). Bearing this in mind, we can specify the conditions under which a Fe^{3+} ion is "isolated" or "clustered" and discuss the variation of the intensity of the ESR signals with y and x (Figs. 2 and 3) in order to obtain more information about the Fe^{3+} distribution.

"Isolated" ions and signal α. The linewidth of the signal α, assigned to isolated ions in the B sites, is larger than that found in other crystalline powders and similar to that observed in amorphous systems (*15*). This is probably due to the local disorder present in our system. In fact the possible presence of a vacancy in a nearby A site changes the symmetry of the crystal field acting on the B site. A variability of the local symmetry of the B sites provokes a variability of the D and E terms, which makes our system similar to an amorphous one.

As far as the number m of cationic B sites which must be free from other Fe^{3+} ions so that a Fe^{3+} occupying it can be considered "isolated," certainly it is higher than four (the number of the n.n. sites).

If a random distribution for Fe^{3+} in the B sites is assumed, the mole fraction, y_0, of the "isolated" Fe^{3+} ions, to which the intensity of the signal α is proportional, is $y_0 = y(1 - y)^m$. This function has a maximum for $y = 1/(1 + m)$. The position of the maximum in the plot of $I\alpha$ vs y then permits the evaluation of m (*9–12*). As shown in Fig. 2, the maximum, although not well defined, can be placed in the range $y = 0.03$–0.05 and then a value in the range 20–30 can be deduced for m. In the B sublattice of the scheelite structure there are 28 cationic sites around a given B site, including the third nearest neighbors, at a distance of ~7.3 Å. This distance is close to those found for Fe^{3+} ions in other oxide systems, namely α-Al_2O_3 (r_0 = 7.4 Å) (*9*), β-Ga_2O_3 (r_0 = 8.0 Å) (*11*), $NaAlO_2$ (r_0 = 8.6 Å) (*10*). This seems to indicate that the range of interaction of the exchange forces is not very dependent on the nature of the oxide matrix holding the Fe^{3+} ions in solid solution (*10*).

"Clustered" ions and signal β. As stated before, there are two types of "clustered" Fe^{3+} ions detected by ESR; the strongly exchange coupled ions in the A–B sites, giving the signal β, and the weakly coupled ions in the B sites, giving the signal γ.

As shown in Fig. 3, the intensity of the signal β depends both on y and x; for a given x, the curve attains a maximum and then tends to zero. Moreover, as x decreases, the maximum is reached at decreasing y values. The trend of these curves can be explained if it is assumed that the A–Ox–B clusters of size higher than a critical value do not contribute to the ESR signal (*9, 11*).

The curves of Fig. 3 therefore indicate that, as x decreases, the critical size of the clusters is reached at lower and lower y values, i.e., that in the samples of series II a nonrandom distribution of Fe^{3+} ions occurs mainly at low x values. On the other hand, since the number of vacant A sites is equal to $(x/3) - y$, one can believe that a high number of vacancies (high value of x) prevents the growth of clusters, so that the critical size is reached at higher y values.

Another manifestation of the same phenomenon (nonrandom distribution) is shown by the dependence of the Weiss tem-

perature θ on y and x (Fig. 4). The Weiss temperature represents in fact a measure of the strength of the antiferromagnetic interactions which depend on the size of the clusters and, obviously, on the type of interaction.

For the molybdovanadate system a nonrandom distribution of the Fe^{3+} ions in the samples of series II means that the occupancy of nearby A and B sites by the Fe^{3+} ions is correlated, i.e., the presence of a Fe^{3+} ion in a B site increases the probability of occupancy of neighboring A sites by other Fe^{3+} ions (Fig. 5). This conclusion explains another feature of the ESR data: the appearance of a rather strong signal β at very low y values. For instance, in the samples with $y = 0.01$ of series II the integrated intensity accounts for about 50% of the iron present, a percentage of two orders of magnitudes higher than that foreseeable for a random distribution.

Model for a quantitative analysis of signal β. In order to hypothesize on the mechanism through which the dispersion of the Fe^{3+} ions occurs in the molybdovanadate system (series II) we shall now perform a quantitative analysis of the curves of Fig. 3.

If the occupancy of nearby A and B sites by Fe^{3+} ions is correlated, i.e., if the substitutional mechanism $Mo_B^{6+} + \square_A \leftrightarrow Fe_B^{3+} + Fe_A^{3+}$ occurs, most of the Fe^{3+} ions exist in pairs, A–Ox–B, and this is also the case at low y values. The number of the Fe_B^{3+}–Ox–Fe_A^{3+} pairs is then proportional to the y parameter, and not to y^2 as for an uncorrelated occupancy. The existence of this strong correlation is probably due to electrostatic effects: in fact the substitution of a Mo^{6+} or V^{5+} ion with a Fe^{3+} ion in a B site strongly perturbs the local electric charge which can partially be compensated by introduction of a small Fe^{3+} ion in one of the eight nearby A sites.

As y increases the Fe_B^{3+}–Ox–Fe_A^{3+} pairs become more and more abundant and therefore their mutual distance decreases, affecting the intensity of the ESR signal. However, since the intensity of the signal β depends on both the y and x parameters, probably the distribution of the above pairs is not totally random, i.e., the clustering of the pairs occurs even at low y values and it depends specifically on x (Fig. 3).

Anyway, regardless of the interpretation, the set of curves in Fig. 3 can be represented, as a first approximation, by a mathematical function of the type: $F_1(x,y) = y[(x/3) - y]$ with $0 \leq y \leq x/3$.

This function represents a set of parabolas, defined by $x/3$ and with the concavity toward the axis of the abscissa; moreover, the function $F_1(x,y)$ reaches its maximum for $y = x/6$, just as the intensity of signal β (Fig. 3), and then goes to zero for $y = x/3$. This last requirement is only partially satisfied by the experimental curves.

By the use of this function it is possible, for each value of x, to evaluate y and $F_1(x,y)$ at the point of maximum. Moreover, since $2y$ represents the iron content, the ratio $(F_1)_{max}/(2y)_{max}$ gives the theoretical fraction of Fe^{3+} contributing to the signal β at the maximum.

The comparison of the experimental ESR data of Fig. 3 with those calculated by the function $F_1(x,y)$, reported in Table 2, shows that this empirical function describes quite well the position of the maximum, but less satisfactorily the relative intensity of signal β (columns 3 and 6 of Table 2) and the fraction of Fe^{3+} ions contributing to the signal β (columns 4 and 7).

Such a function, however, has an important physical meaning which sheds some light on the mechanism by which the dispersion of Fe^{3+} occurs into the scheelite structure, and it also helps to search for a better function.

Recalling in fact that $[(x/3) - y]$ is the concentration of the vacancies in A sites and y, with the assumptions made before, represents the concentration of the Fe_B^{3+}–Ox–Fe_A^{3+} pairs, the function $F_1(x,y) = y[(x/3) - y]$ computes the probability of occurrence of the association vacancy-pair, in the case of a random (noncorrelated) distribution of these two entities.

TABLE 2

Quantitative Analysis of Signal β by Comparison of ESR Data of Fig. 3 with Those Evaluated with Help of Two Empirical Functions: $F_1(x,y) = y[(x/3) - y]$; $F_2(x,y) = 7y[(x/3) - y] \cdot [1 - (x/3) + y]^6$

x	Experimental data of Fig. 3			Values calculated by the functions:					
				$F_1(x,y)$			$F_2(x,y)$		
	y_{max}[a]	$\frac{I_{\beta,max}}{I^{\circ}_{\beta,max}}$[b]	Fraction of Fe at y_{max}	y_{max}[a]	$\frac{F_{1,max}}{F^{\circ}_{1,max}}$[c]	$\frac{F_{1,max}}{2y_{max}}$	y_{max}[a]	$\frac{F_{2,max}}{F^{\circ}_{2,max}}$[c]	$\frac{F_{2,max}}{2y_{max}}$
0.75	0.15	1.00	0.14	0.125	1.00	0.062	0.170	1.00	0.170
0.60	0.10	0.72	0.15	0.100	0.64	0.050	0.129	0.71	0.160
0.45	0.09	0.63	0.15	0.075	0.36	0.037	0.092	0.45	0.142
0.30	0.05	0.29	0.13	0.050	0.16	0.025	0.058	0.23	0.114
0.15	0.025	0.06	0.05	0.025	0.04	0.012	0.027	0.06	0.070

[a] y_{max}: value of y parameter at maximum.
[b] $I^{\circ}_{\beta,max}$: intensity of β signal at maximum for the specimen with $x = 0.75$.
[c] $F^{\circ}_{1,max}$, $F^{\circ}_{2,max}$: values of $F_1(x,y)$ and $F_2(x,y)$ at maximum for the specimen with $x = 0.75$.

However, since each A–Ox–B cation pair has seven n.n. A sites (Fig. 5) in which a vacancy can be found, the probability of occurrence of a Fe^{3+}_B–Ox–Fe^{3+}_A pair associated with a vacancy is then $F_2(x,y) = 7y[(x/3) - y] \cdot [1 - (x/3) + y]^6$.

The function $F_2(x,y)$ represents quite well the experimental ESR data of Fig. 3; a comparison between calculated and experimental results is given in Table 2.

We believe that this excellent agreement is not merely fortuitous but that it is a good indication that the vacancies in the A sites are the main factor controlling the growth of the size of the Fe^{3+} clusters; in fact, when the probability of occurrence of a vacant A site associated with Fe^{3+}_B–Ox–Fe^{3+}_A pair, i.e., $F_2(x,y)$, begins to decrease, the intensity of signal β goes down (Fig. 3) and the Weiss temperature θ strongly increases (Fig. 4), indicating that, at the same time, the size of the iron clusters grows.

It follows that the content of vacancies, clearly depending on the molydenum content, controls not only the incorporation but even more the distribution and dispersion of iron in both A and B sites of the scheelite, according to the general formula of the bismuth molybdovanadate iron-containing system.

CONCLUSIONS

The main conclusions which can be drawn from the magnetic and ESR data of this work are as follows:

(i) The X-ray results (*1*), which interpreted the incorporation and distribution of Fe^{3+} ions in the B or in the A and B sites of scheelite, and which led to the classification of the samples in the two series I and II, are confirmed.

(ii) The substitution of one Mo^{6+} ion (in the B site) and one vacancy (in the A site) with two Fe^{3+} ions (series II) occurs with a correlated distribution, leading to the Fe^{3+}_B–Ox–Fe^{3+}_A couple.

(iii) In the samples of series II strong antiferromagnetic interactions of A–Ox–B type arise with the y parameter; the behavior of the Weiss temperature θ parallels that of the ESR signal β, and both depend on the size of Fe^{3+} clusters.

(iv) The content of vacancies, $\square = [(x/3) - y]$, not only controls the solubility of iron (Fe = y) in the scheelite structure, but it also strongly affects the growth of the iron clusters size.

ACKNOWLEDGMENTS

The authors would like to thank Professor A.

Cimino for critically reading of the manuscript, and Mr. M. Inversi for making the drawings.

REFERENCES

1. Porta, P., Lo Jacono, M., Valigi, M., Minelli, G., Anichini, A., De Rossi, S., and Gazzoli, D., *J. Catal.* **100,** 86 (1986).
2. Ja, Y. H., *J. Chem. Phys.* **57,** 3020 (1972).
3. Aasa, R., *J. Chem. Phys.* **52,** 3919 (1970).
4. Castner, T., Newell, G. S., Holton, W. C., and Slichter, C. P., *J. Chem. Phys.* **32,** 668 (1960).
5. Dowsing, R. D., and Gibson, J. F., *J. Chem. Phys.* **50,** 294 (1969).
6. Poole, C. P., and Itzel, I. F., *J. Chem. Phys.* **41,** 287 (1964).
7. Strombler, M. P., Farch, H. A., and Poole, C. P., *Phys. Rev. B: Condens. Matter* **6,** 40 (1971).
8. Carman, C. J., and Kroenke, W. J., *J. Phys. Chem.* **72,** 2562 (1968).
9. Gesmundo, F., and De Asmundis, C., *J. Phys. Chem. Solids* **33,** 1861 (1972).
10. Gesmundo, F., and De Asmundis, C., *Ann. Chim.* **63,** 655 (1973).
11. Gesmundo, F., and De Asmundis, C., *J. Phys. Chem. Solids* **34,** 637 (1973).
12. Gesmundo, F., and Rossi, P. F., *J. Solid State Chem.* **8,** 287, 297 (1973).
13. Korteweg, G. A., and van Reyen, L. L., *J. Magn. Res.* **44,** 159 (1981).
14. Fournier, J. T., Landry R. L., and Bartram, R. H., *J. Chem. Phys.* **55,** 2522 (1971).
15. Bogomolova, L. D., and Henner, E. K., *J. Magn. Res.* **41,** 422 (1980).
16. Gulley, J. E., Hone, D., Scalapino, D. J., and Silbernogel, B. G., *Phys. Rev. B: Condens. Matter* **1,** 1020 (1970).
17. Sleight, A. W., "Advanced Materials in Catalysis," pp. 181–208. Academic Press, New York, 1977; Jeitschko, W., Sleight, A. W., McClellan, W. R., and Weiher, J. F., *Acta Crystallogr Sect. B* **32,** 1163 (1976); Colombo, A., and Zocchi M., private communication; and other references in these papers.